

Low energy magnetic radiation enhancement in the $f_{7/2}$ shell

S. Karampagia, B. A. Brown and V. Zelevinsky

*National Superconducting Cyclotron Laboratory and Department of Physics and Astronomy,
Michigan State University, East Lansing, MI 48824-1321, USA*

Studies of the γ -ray strength functions can reveal useful information concerning underlying nuclear structure. Accumulated experimental data on the strength functions show an enhancement in the low γ energy region. We have calculated the M1 strength functions for the $^{49,50}\text{Cr}$ and ^{48}V nuclei in the $f_{7/2}$ shell-model basis. We find a low-energy enhancement for gamma decay similar to that obtained for other nuclei in previous studies, but for the first time we are also able to study the complete distribution related to M1 emission and absorption. We find that M1 strength distribution peaks at zero transition energy and falls off exponentially. The height of the peak and the slope of the exponential are approximately independent of the nuclei studied in this model space and the range of initial angular momenta. We show that the slope of the exponential fall off is proportional to the energy of the $T = 1$ pairing gap.

I. INTRODUCTION

In order to understand the nuclear properties in the quasicontinuum, statistical quantities are used, such as the nuclear level density and the γ -ray strength function (γSF) [1] for a particular multipolarity. The strength function is the average reduced radiation or absorption probability of photons of given energy E_γ . It is commonly adopted that the E1 strength function is dominated by the giant electric dipole resonance (GDR) around $E_\gamma \approx 78 \cdot A^{-1/3}$ MeV, which can be reproduced, not too far from the maximum, by a classical Lorentz line [2, 3]. It was earlier assumed that the E1 strength function for lower energy γ -rays corresponds to the tail of this Lorentzian. Current experimental data [4, 5] show that the Lorentzian description fails for these energies. In order to account for the lower γ energies, the Kadmen'skii- Markusev-Furman (KMF) model [6] was suggested. Empirical modifications of this model [7] have also been used to describe the behavior of the E1 strength function at low E_γ with the use of the temperature-dependent GDR width.

Experimentally, resonances in the low E_γ region have long been observed, commonly termed as pygmy dipole resonances and attributed to the enhancement of the E1 strength function [8], partly due to the presence of a neutron skin. Recent studies in rare earth nuclei have shown [9, 10] that bumps in the $E_\gamma \approx 3$ MeV region are of M1 character. Actually, the M1 transitions seem to play an active role in the γSF being described also by a Lorentz line [11] based on the existence of a resonance that originates from spin-flip excitations in the nucleus [12, 13].

In the last decade things have become more complicated, since measurements of the γSF [10, 14–26] have revealed a newly observed minimum around $E_\gamma \simeq 2 - 4$ MeV, so besides the high E_γ enhancement, there is also a low E_γ enhancement. The first attempts to understand the low- E_γ enhancement [14, 15, 17] used the KMF model to describe the GDR; the contribution of the giant magnetic dipole resonance to the total γSF is fitted by a Lorentzian, similarly to the E2 resonance, while the

low- E_γ region is described by a separate term that has a power-law parametrization. In [19] the authors used a functional form of the γSF with contributions from E1 and M1 resonances plus an exponential low-energy enhancement function to simulate two-step γ -cascade spectra. They found that all M1 strength functions show a low- E_γ increase compared to the uncertain behavior of the low-energy E1 strength functions.

In [23, 25] it was found that the E2 transitions are of minor importance whereas the dipole transitions dominate in the low- E_γ enhancement region. The first theoretical evidence of the strong enhancement at low E_γ came from the shell model calculations of $B(\text{M1})$ values for ^{90}Zr , $^{94-96}\text{Mo}$ [22] and $^{56,57}\text{Fe}$ [27] where the calculated $B(\text{M1})$ and the γSF showed large values for low E_γ . The influence of this low energy enhancement of the γSF is not of minor importance, as it has been found that the neutron capture reaction rates can grow due to this effect by 1-2 orders of magnitude [28].

In this study, we calculate $B(\text{M1})$ for ^{49}Cr , ^{50}Cr , and ^{48}V in the model space of $f_{7/2}$ using the OXBASH shell model code [29]. Although the model space is small, the results lead to new insights. In addition, we are able to consider the M1 strength for transitions to excited states (γ absorption). From this we show for the first time that the low-energy part of the M1 distribution is peaked at zero energy, and falls off exponentially below and above that point. For these nuclei we consider the states with $T = T_z$ obtained with the F742 Hamiltonian from [30] that reproduces the known low-lying energies in the nuclei of interest. The results are largely independent of the nucleus, the range of initial spins and the excitation energy. We show that the slope of the exponential fall off is determined mainly from the $T = 1$ (pairing) part of the Hamiltonian.

In the discussion we compare the M1 strength results for the $f_{7/2}$ model space with those obtained from the full pf model space for ^{48}V , again for states with $T = T_z$. By allowing the successive occupance of all the orbitals of the pf shell, starting with the $f_{7/2}$ orbital alone, we explore how the addition of orbitals affects the low-energy enhancement and the overall M1 strength distribution.

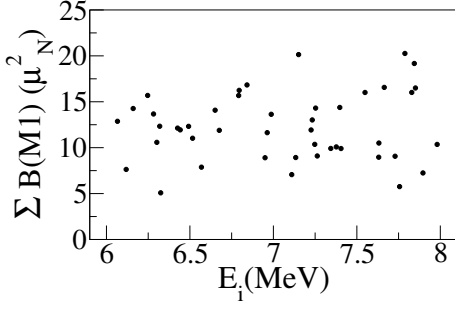


FIG. 1: Summed $B(M1)$ strength for a range of initial states in ^{50}Cr .

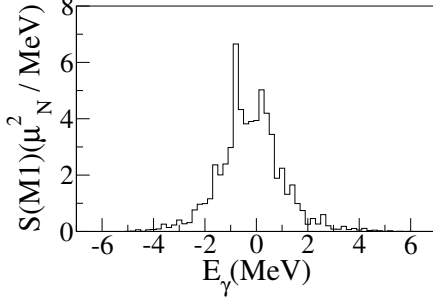


FIG. 2: The average M1 strength distribution for states between 6 and 8 MeV in ^{50}Cr .

We also compare our results to the available experimental M1 strength function of ^{50}V .

II. RESULTS

We start by considering the states in ^{50}Cr from 6 to 8 MeV. The sum of $B(M1)$ s stemming from each initial state is shown in Fig. 1. This has a Porter-Thomas type scatter around an average value of $12.5 \mu_N^2$. The average M1 strength distribution $S(M1)$ is shown in Fig. 2. This is obtained by first sorting the $B(M1)$ s according to the increasing energy differences, $E_\gamma = E_i - E_f$ and summing them over bins of $\Delta E_\gamma = 0.2$ MeV, for a certain initial energy range (here $E_i = 6-8$ MeV). These are then averaged over the number of initial states,

$$S_i = \frac{\sum_{\text{bins}} B(M1)_{\{E_i=6-8\text{MeV}\}}}{\text{Number of initial states}}. \quad (1)$$

The area of the $S(M1)$ in Fig. 2 is $12.5 \mu_N^2$.

Experimentally, the quantity of interest is the γ decay strength function γSF defined by [1]

$$f_{\text{ML}}^i(E_\gamma) = \rho_i \frac{\langle \Gamma_{\gamma i}(E_\gamma) \rangle}{E_\gamma^{2L+1}}, \quad (2)$$

where L characterizes the multipolarity of the transition and ρ_i is the level density of the initial states. The partial

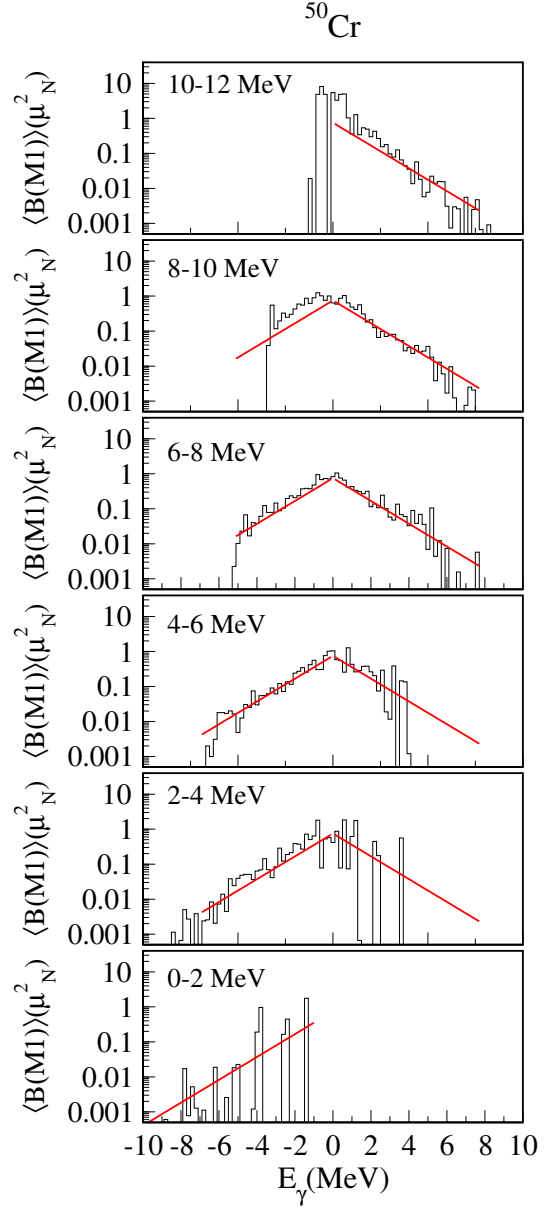


FIG. 3: Average $B(M1)$ values as a function of γ -ray energy E_γ for ^{50}Cr and initial energies, E_i , in various 2 MeV ranges. The lowest panel is for 0-2 MeV, the highest for 10-12 MeV. Each M1 distribution is compared to the same exponential, red line, with parameters $B_0 = 0.75 \mu_N^2$ and $T_B = 1.33$ MeV.

radiative width Γ_γ is given, for M1 transitions, by

$$\Gamma_{\gamma i, M1}(E_\gamma) = \frac{16\pi}{9} \left(\frac{E_\gamma}{\hbar c} \right)^3 B(M1)(E_\gamma)_i, \quad (3)$$

where the index i specifies selected initial spin values and the initial energy region E_i . By combining the two expressions we find the γSF ,

$$f_{M1}(E_\gamma) = a \langle B(M1)(E_\gamma) \rangle_i \rho_i(E_i), \quad (4)$$

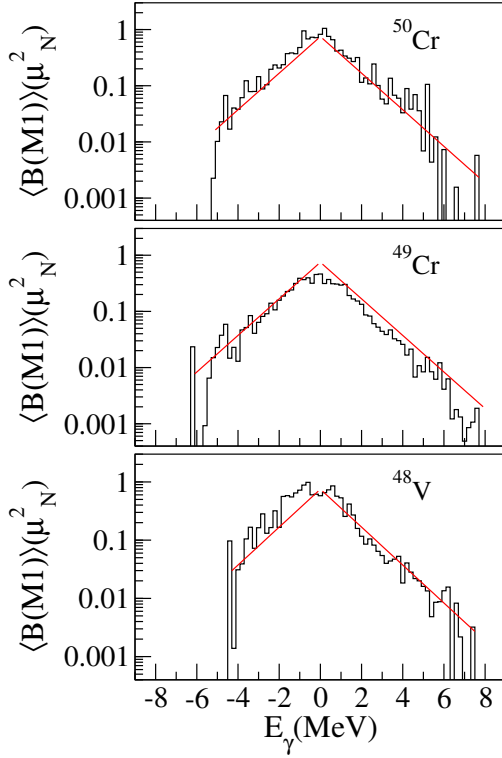


FIG. 4: Average $B(M1)$ values as a function of γ -ray energy E_γ for ^{49}Cr , ^{50}Cr , and ^{48}V for initial energies, E_i , in the interval 6-8 MeV. Each M1 distribution is compared to the same exponential, red line, with parameters $B_0 = 0.75 \mu_N^2$ and $T_B = 1.33$ MeV.

where

$$a = \frac{16\pi}{9(\hbar c)^3} = 11.5473 \cdot 10^{-9} \mu_N^{-2} \cdot \text{MeV}^{-2}. \quad (5)$$

We will show the results in terms of the $\langle B(M1)(E_\gamma) \rangle$ of Eq. (4). At the end we will consider the γSF . The calculated $B(M1)$ values are sorted according to increasing transition energy, E_γ , and grouped in energy bins of 0.2 MeV width. For each bin the average $B(M1)$ value, $\langle B(M1)(E_\gamma) \rangle$, was found by dividing the sum of the $B(M1)$ values in this bin by their number. This leads to a plot whose average value at a given E_γ does not depend on the bin size.

The results for ^{50}Cr are shown in Fig. 3 for several ranges of initial energies. The straight lines shown in all panels are for the exponents, $B_0 e^{-|E_\gamma|/T_B}$, with $B_0 = 0.75 \mu_N^2$ and $T_B = 1.33$ MeV (the notation of reference [22] is used). A similar exponential behavior is seen in all regions of excitation energy, even for the lowest region of 0 to 2 MeV, where only γ absorption can take place. This result is very different from the Brink-Axel model where the strength function on excited states is related to the absorption strength function in the ground state. In contrast, the low-energy distribution is a generic feature for excited states, that cannot be obtained from information on the ground state since it peaks at zero

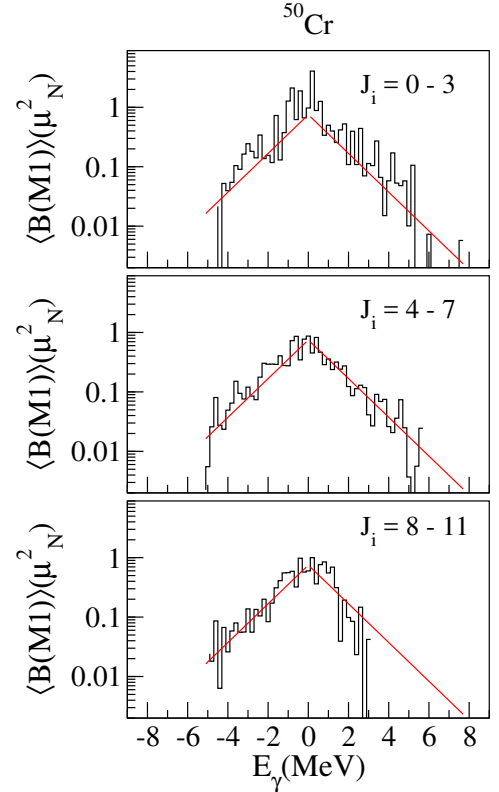


FIG. 5: Average $B(M1)$ values for ^{50}Cr as a function of γ -ray energy, E_γ , for different initial spin ranges. Each M1 distribution is compared to the same exponential, red line, with parameters $B_0 = 0.75 \mu_N^2$ and $T_B = 1.33$ MeV.

energy.

Comparative $B(M1)$ diagrams for all three nuclei at $E_i = 6-8$ MeV can be seen in Fig. 4. They all have essentially the same functional form. The results for ^{50}Cr divided into different ranges for the initial spin are shown in Fig. 5. The exponential shape is independent of spin.

In our orbital space, the two-body interaction Hamiltonian has only eight non-zero matrix elements, four for the isospin $T = 0$ pairs and four for $T = 1$. By following the procedure of [31], we divide the Hamiltonian into two parts and, keeping the symmetry, let them vary through the numerical coefficients, k_0 and k_1 ,

$$H = h + k_0 V(T=0) + k_1 V(T=1), \quad (6)$$

where the part h contains the single-particle energies, $V(T=0)$ includes the matrix elements with $T=0$ while $V(T=1)$ includes the matrix elements with $T=1$. The absence of the $T=1$ matrix elements, (mainly pairing, $J^\pi T = 0^+ 1$ and $J^\pi T = 2^+ 1$), makes the spectrum collapse to low energies. We find that the shape of the M1 distribution depends very little on the $T=0$ interaction, as shown in Fig. 6, but there is a strong dependence on the strength of the $T=1$ interaction.

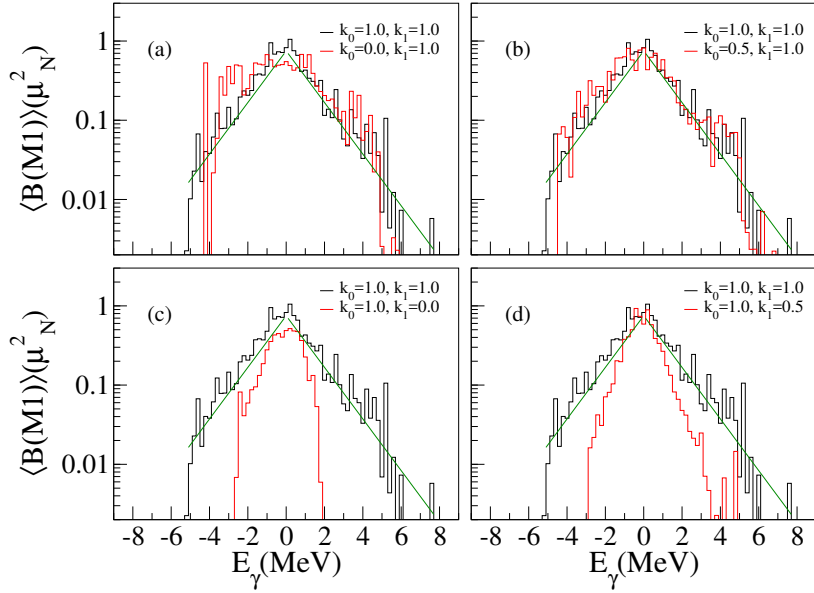


FIG. 6: Average $B(M1)$ values as a function of γ -ray energy E_γ (black line) for ^{50}Cr for initial energy, E_i , in the interval 6-8 MeV, compared with the average $B(M1)$ values derived using (a) $k_0=0.0$, $k_1=1.0$, (b) $k_0=0.5$, $k_1=1.0$, (c) $k_0=1.0$, $k_1=0.0$, (d) $k_0=1.0$, $k_1=0.5$, red line. The green line is the exponential fit with $B_0 = 0.75 \mu_N^2$, $T_B = 1.33$ MeV.

III. DISCUSSION

For the case of the nuclei studied, it is found that the slope, T_B , of the exponential functions fitted on the $\langle B(M1)(E_\gamma) \rangle$, is almost constant for all nuclei, while the height seems to vary more, depending on the nucleus. A closer look in Fig. 4 shows that the selected B_0 value of the preexponent for ^{49}Cr slightly overestimates the $\langle B(M1)(E_\gamma) \rangle$ function; however, the choice of a common B_0 value for these nuclei gives a good description of the $\langle B(M1)(E_\gamma) \rangle$.

The approximation of the M1 strength by an exponential function has already been proposed in [22]. There, the $\langle B(M1)(E_\gamma) \rangle$ was calculated using the shell model for $^{94,95,96}\text{Mo}$ and ^{90}Zr , in a model space which permits both positive and negative parity states. The slope of the exponential for the positive parity states ranges from $T_B=(0.33-0.41)$ MeV, the lowest value corresponding to ^{90}Zr . The slope of the negative parity states ranges from $T_B=(0.50-0.58)$ MeV for the Mo isotopes, while $T_B=0.29$ MeV for ^{90}Zr [22]. The slope for both parities is much more steep than the one found in this study.

The difference in the exponential slopes in the two studies can be attributed to the different orbitals used for the studied nuclei. In our calculations we know that it is only the $f_{7/2}$ orbital that contributes to the low-energy enhancement, but we don't know which are the important orbitals for [22]. From the text it seems that these are the $g_{9/2}$ and $d_{5/2}$, but no further conclusions can be drawn. However, we can say that the use of different orbitals will give rise to different slopes. Another thing that could be affecting the slope of the low-energy enhancement, is the masses of the studied nuclei. As has already

been shown, the pairing interaction is the main factor that affects the M1 distribution. The pairing changes the slope of the $\langle B(M1)(E_\gamma) \rangle$, in a way that, less pairing, gives a steeper slope. Pairing depends on A by a factor of $\alpha_p/A^{1/2}$ [32], so in the $A=90-96$ region, pairing is 25% smaller than the $A=48-50$, thus the slope of the M1 distribution will be steeper.

In order to explore the point that the consideration of different orbitals will give rise to different slopes, we present in Figs. 7-8 the calculated γSF of ^{48}V from Eq. (4), using the $f_{7/2}$ model space (black dashed stair line) and the GX1A interaction [33, 34] in the pf model space, allowing successively different orbitals to be added to the model space. In Fig. 7 we first allow only the $f_{7/2}$ orbital to be occupied (red dot stair line), then the $f_{7/2}, f_{5/2}$ (blue heavy stair line) and $f_{7/2}, p_{3/2}, f_{5/2}$ (green double dot - dash stair line) orbitals; finally we compare with the full pf calculation (orange stair line). In Fig. 8 we give a different sequence of occupied orbitals in the pf model space, starting again with the $f_{7/2}$ orbital (red dot stair line), but then allowing the $f_{7/2}, p_{3/2}$ (violet heavy stair line) and $f_{7/2}, p_{3/2}, p_{1/2}$ (purple double dot - dash stair line) orbitals to be occupied. We chose to study the γSF on ^{48}V because it is the closer nucleus to the available experimental γSF measurements for ^{50}V .

We notice that the full pf shell calculation is more flat compared to the $f_{7/2}$ model space or the pf shell calculation, when only the $f_{7/2}$ orbital is occupied. In both Figs. 7 and 8, the successive allowance of occupancy of a new orbital makes the γSF distribution to drop, up until $E_\gamma \sim 2$ MeV. For $2 < E_\gamma < 4$ MeV, the distributions from different occupancies (except the full pf calculation) are almost identical. In Fig. 7 we see that

the presence of the $f_{5/2}$ orbital affects the spectrum for $E_\gamma > 4$ MeV, as it gives a spin-flip term which is observed as a peak in the γ emission strength, around $E_\gamma = 6-8$ MeV. This energy comes from the spin-orbit $f_{7/2} - f_{5/2}$ splitting. The addition of more orbitals in the pf model space doesn't change the γ SF for $E_\gamma > 4$ MeV. The effects of the $f_{5/2}$ orbital can be easily observed in Fig. 7 as well. There, the successive addition of the $p_{3/2}$ and $p_{1/2}$ occupancies doesn't change the γ SF for $E_\gamma > 2$ MeV. However, the addition of the last orbital, $f_{5/2}$, is immediately understood, as the γ SF distribution increases for $E_\gamma > 4$ MeV. The small differences observed for the $f_{7/2}$ model space and the pf shell calculation, truncated to the $f_{7/2}$ orbital, are attributed to the differences in the interactions, as well as the mass dependence present in the GX1A interaction.

The mixing of the different orbitals with the diagonal $f_{7/2}$ will quench the low-energy strengths discussed in this study. However, it is mainly the diagonal $f_{7/2}$ part which gives the low-energy enhancement of the strength function. This can also be confirmed by the single-particle occupation numbers of the full pf shell calculation. We see that protons and neutrons mainly occupy the $f_{7/2}$ single-particle level, the rest of the orbitals having considerably smaller occupation numbers.

A different example of how the mixing of orbitals can affect the M1 strength function can be seen in Fig. 9. There, besides the ^{48}V calculations using the full pf and $f_{7/2}$ model spaces, we also show the M1 strength function of ^{56}Fe , using a truncated pf space, $(0f_{7/2})^{6-t}(0f_{7/2}, 1p_{3/2}, 1p_{1/2})^t$ for protons and $(0f_{7/2})^{8-t}(0f_{7/2}, 1p_{3/2}, 1p_{1/2})^{t+n}$ for neutrons, where $n = 2$ and $t = 0, 1$ and 2 [27]. We see that the slope of the exponential for $E_\gamma \leq 2$ MeV is steeper than the full pf space calculation for ^{48}V , but similar to the ^{48}V $f_{7/2}$ model space calculation. Further investigation needs to be done on how a truncated model space affects the M1 strength function distribution in order to fully understand the difference in the slopes of the pf calculations.

The results for the ^{48}V γ SF in the pf space (black dashed stair line), along with the available experimental data for ^{50}V (red circles and blue down triangles), are shown in Fig. 10. These data are reanalyzed [35] and renormalized to new neutron-resonance data and new spin distributions. As neutron-resonance data on ^{50}V are not available (since ^{49}V is unstable), the systematics in this mass region and lower/upper limits for ^{51}V have been used as constraints. The upper limit of the ^{50}V experimental data agrees better with the theoretical calculations. The lack of experimental data below $E_\gamma = 1.75$ MeV makes the comparison with theory difficult in this important region. The γ SFs calculated using the $f_{7/2}$ model space is only added for demonstration reasons. As was noted in Figs. 7-8, the $f_{7/2}$ model space cannot be used for comparison with the experiment due to the lack of the other orbitals, which play also a significant role to the formation of the strength distribution, however it can be used to clarify certain physical aspects

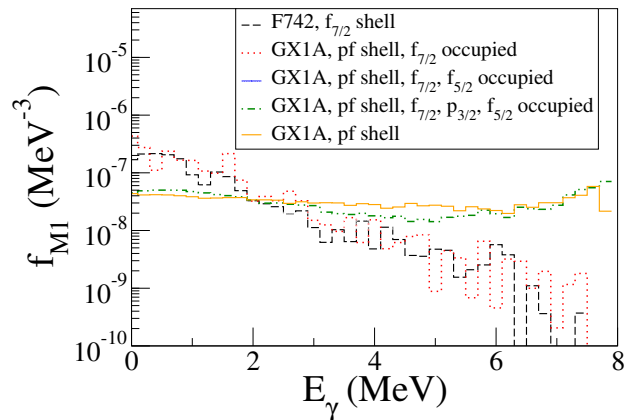


FIG. 7: Calculated γ SF values for ^{48}V using the $f_{7/2}$ model space (black dashed stair line) and the GX1A interaction in the pf model space allowing first the $f_{7/2}$ orbital to be occupied (red dot stair line), then the $f_{7/2}, f_{5/2}$ (blue heavy stair line), the $f_{7/2}, p_{3/2}, f_{5/2}$ (green double dot - slash stair line) orbitals and last all the pf shell (orange stair line), as a function of γ -ray energy, E_γ , for initial energies, E_i , in the interval 6-8 MeV.

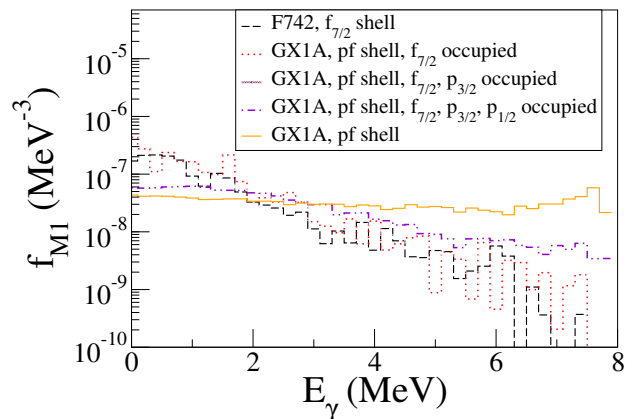


FIG. 8: Calculated γ SF values for ^{48}V using the $f_{7/2}$ model space (black dashed stair line) and the GX1A interaction in the pf model space allowing first the $f_{7/2}$ orbital to be occupied (red dot stair line), then the $f_{7/2}, p_{3/2}$ (violet heavy stair line), the $f_{7/2}, p_{3/2}, p_{1/2}$ (purple double dot - slash stair line) orbitals and last all the pf shell (orange stair line), as a function of γ -ray energy, E_γ , for initial energies, E_i , in the interval 6-8 MeV.

of the γ SF.

The exponential form seems to be generic for the problems where we have a bilinear combination of more or less random operators. An analog can be found in the statistical distribution for off-diagonal matrix elements of a realistic many-body Hamiltonian used in the full shell-model calculations in a finite orbital space. It was studied in detail for an example of the sd shell model long ago [37], see Figs. 8 and 9 and the Appendix there. Contrary to standard embedded ensembles of random matrices with Gaussian-like distribution of matrix elements

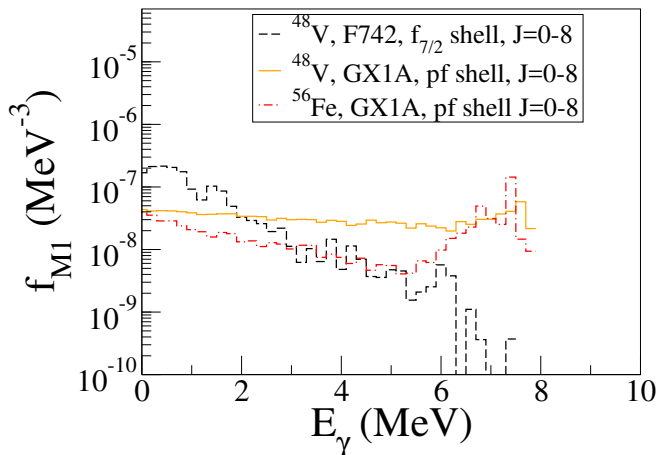


FIG. 9: Calculated γ SF values for ^{48}V in the $f_{7/2}$ (black dashed stair line) and the pf (orange solid line) model spaces compared to the γ SF values for ^{56}Fe in the pf (red dot dash stair line) model space, as a function of γ -ray energy, E_γ , for initial energies, E_i , in the interval 6-8 MeV.

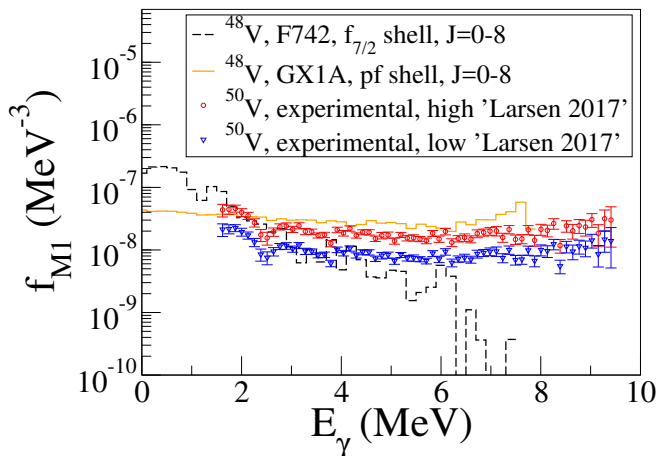


FIG. 10: Calculated γ SF values for ^{48}V in the $f_{7/2}$ (black dashed stair line) and the pf (orange solid line) model spaces compared to the experimental low limit (blue down triangles) and high limit (red circles) data of ^{50}V (Larsen 2017: [35]), as a function of γ -ray energy, E_γ , for initial energies, E_i , in the interval 6-8 MeV.

[38], in such practical applications we typically have a distribution close to the exponential, maybe with some prefactors (mostly important for the smallest matrix elements). This situation supposedly emerges when the random quantities are matrix elements of multipole operators while the main terms of the many-body Hamiltonian are their bilinear combinations like multipole-multipole forces. Similar to the Porter-Thomas, or more general chi-square, case, the distributions of the bilinear combinations are mainly exponential. The exponential factor, as the effective temperature above, can be roughly estimated as the mean (over the spectrum) excitation energy characteristic for the multipole operator. In our small or-

bital space, the spin-orbital and monopole terms are reduced to constants. The effective Hamiltonian governed by the pairing-type interaction contains also less coherent parts creating actual superpositions corresponding to complicated stationary states. The diagonal in seniority matrix elements of a time-odd operator, such as the magnetic moment, are not renormalized by pairing. This corresponds to the maximum strength at small E_γ . For the components changing the seniority the mean transition energy is of the order of the pairing gap Δ equal to about 1.5 MeV for this group of nuclei. This estimate agrees with the effective temperature T_B found above.

This physics cannot satisfy the Brink-Axel hypothesis which can be approximately valid for the excitations of general macroscopic nature. In the GDR case, the main part is played by the local dipole polarization of the nuclear medium which is essentially a universal property of nuclear matter. Such an excitation can be erected on top of any shell-model state. In the case considered above, low-energy properties, such as isovector pairing and spin-orbit splitting of specific single-particle orbitals, are crucial.

IV. CONCLUSION

Summarizing, we have performed shell-model calculations in the $f_{7/2}$ shell, producing the full spectra and decay schemes of ^{48}V , ^{49}Cr , and ^{50}Cr . The results indicate a strong low- E_γ $B(M1)$ component, in accordance with experimental and theoretical findings. The new outcome of this study is that the low energy enhancement is essentially a one-partition phenomenon. Also, it is practically independent of the initial energy window or the spin distribution considered. All the $B(M1)$ functions can be well fitted as exponential, while it is shown that it is the $T = 1$ matrix elements which are responsible for the exponential shape (the $T = 0$ matrix elements provide a very small bump at low energies). The comparison of the calculations of the γ SF in the $f_{7/2}$ and the full pf shell model space, as well as for the successive occupation of different orbitals in the pf model space, suggests that the mixing of different orbitals with the $f_{7/2}$ leads to the quenching of the low-energy enhancement. The $f_{5/2}$ orbital has a special role, as it gives a spin-flip peak at $E_\gamma = 6-8$ MeV. The role of spin-orbital interactions should be studied in more detail.

Acknowledgements

We acknowledge support from NSF grant PHY-1404442.

-
- [1] G. A. Bartholomew, E. D. Earle, A. J. Ferguson, J. W. Knowles, and M. A. Lone, *Adv. Nucl. Phys.* **7**, 229 (1973).
- [2] P. Axel, *Phys. Rev.* **126**, 671 (1962).
- [3] B. L. Berman and S. C. Fultz, *Rev. Mod. Phys.* **47**, 713 (1975).
- [4] Yu. P. Popov, *Sov. J. Part. Nucl.* **13**, 483 (1982).
- [5] A. Voinov, M. Guttormsen, E. Melby, J. Rekstad, A. Schiller, and S. Siem, *Phys. Rev. C* **63**, 044313 (2001).
- [6] S. G. Kadenskii, V. P. Markushev, and V. I. Furman, *Sov. J. Nucl. Phys.* **37**, 165 (1983).
- [7] J. Kopecky and M. Uhl, *Phys. Rev. C* **41**, 1941 (1990).
- [8] M. Igashira, H. Kitazawa, M. Shimizu, H. Komano, and N. Yamamuro, *Nucl. Phys.* **A457**, 301 (1986).
- [9] M. Krtićka, F. Bečvář, J. Honzátko, I. Tomandl, M. Heil, F. Käppeler, R. Reifarth, F. Voss, and K. Wisshak, *Phys. Rev. Lett.* **92**, 172501 (2004).
- [10] A. Simon, M. Guttormsen, A. C. Larsen, C. W. Beausang, P. Humby, J. T. Burke, R. J. Casperson, R. O. Hughes, T. J. Ross, J. M. Allmond, R. Chyzh, M. Dag, J. Koglin, E. McCleskey, M. McCleskey, S. Ota, and A. Saastamoinen, *Phys. Rev. C* **93**, 034303 (2016).
- [11] J. Kopecky, M. Uhl, and R. E. Chrien, *Phys. Rev. C* **47**, 312 (1993).
- [12] A. Bohr and B.R. Mottelson, *Nuclear Structure*, Vol. II: Nuclear Deformations, p. 638 (World Scientific, 1998).
- [13] K. Heyde, P. von Neumann-Cosel, and A. Richter, *Rev. Mod. Phys.* **82**, 2365 (2010).
- [14] A. Voinov, E. Algin, U. Agvaanluvsan, T. Belgia, R. Chankova, M. Guttormsen, G. E. Mitchell, J. Rekstad, A. Schiller, and S. Siem, *Phys. Rev. Lett.* **93**, 142504 (2004).
- [15] M. Guttormsen, R. Chankova, U. Agvaanluvsan, E. Algin, L. A. Bernstein, F. Ingebretsen, T. Lönnroth, S. Messelt, G. E. Mitchell, J. Rekstad, A. Schiller, S. Siem, and A. C. Sunde, A. Voinov, S. Ødegård, *Phys. Rev. C* **71**, 044307 (2005).
- [16] A. C. Larsen, R. Chankova, M. Guttormsen, F. Ingebretsen, S. Messelt, J. Rekstad, S. Siem, N. U. H. Syed, S. W. Ødegård, T. Lönnroth, A. Schiller, and A. Voinov, *Phys. Rev. C* **73**, 064301 (2006).
- [17] A. C. Larsen, M. Guttormsen, R. Chankova, F. Ingebretsen, T. Lönnroth, S. Messelt, J. Rekstad, A. Schiller, S. Siem, N. U. H. Syed, and A. Voinov, *Phys. Rev. C* **76**, 044307 (2007).
- [18] E. Algin, U. Agvaanluvsan, M. Guttormsen, A. C. Larsen, G. E. Mitchell, J. Rekstad, A. Schiller, S. Siem, A. Voinov, *Phys. Rev. C* **78**, 054321 (2008).
- [19] A. Voinov, S. M. Grimes, C. R. Brune, M. Guttormsen, A. C. Larsen, T. N. Massey, A. Schiller, and S. Siem, *Phys. Rev. C* **81**, 024319 (2010).
- [20] A. Bürger, A. C. Larsen, S. Hilaire, M. Guttormsen, S. Harissopulos, M. Kmiecik, T. Konstantinopoulos, M. Krtićka, A. Lagoyannis, T. Lönnroth, K. Mazurek, M. Norrby, H. T. Nyhus, G. Perdikakis, S. Siem, A. Spyrou, and N. H. U. Syed, *Phys. Rev. C* **85**, 064328 (2012).
- [21] M. Wiedeking, L. A. Bernstein, M. Krtićka, D. L. Bleuel, J. M. Allmond, M. S. Basunia, J. T. Burke, P. Fallon, R. B. Firestone, B. L. Goldblum, R. Hatarik, P. T. Lake, I.-Y. Lee, S. R. Leshner, S. Paschalis, M. Petri, L. Phair, and N. D. Scielzo, *Phys. Rev. Lett.* **108**, 162503 (2012).
- [22] R. Schwengner, S. Frauendorf, and A. C. Larsen, *Phys. Rev. Lett.* **111**, 232504 (2013).
- [23] A. C. Larsen, N. Blasi, A. Bracco, F. Camera, T. K. Eriksen, A. Görgen, M. Guttormsen, T. W. Hagen, S. Leoni, B. Million, H. T. Nyhus, T. Renström, S. J. Rose, I. E. Ruud, S. Siem, T. Tornyi, G. M. Tveten, A. V. Voinov, and M. Wiedeking, *Phys. Rev. Lett.* **111**, 242504 (2013).
- [24] F. Giacoppo, F. L. Bello Garrote, L. A. Bernstein, D. L. Bleuel, R. B. Firestone, A. Görgen, M. Guttormsen, T. W. Hagen, M. Klintefjord, P. E. Koehler, A. C. Larsen, H. T. Nyhus, T. Renström, E. Sahin, S. Siem, and T. Tornyi, *Phys. Rev. C* **91**, 054327 (2015).
- [25] A. C. Larsen, M. Guttormsen, R. Schwengner, D. L. Bleuel, S. Goriely, S. Harissopulos, F. L. Bello Garrote, Y. Byun, T. K. Eriksen, F. Giacoppo, A. Görgen, T. W. Hagen, M. Klintefjord, T. Renström, S. J. Rose, E. Sahin, S. Siem, T. G. Tornyi, G. M. Tveten, A. V. Voinov, and M. Wiedeking, *Phys. Rev. C* **93**, 045810 (2016).
- [26] T. Renström, H.-T. Nyhus, H. Utsunomiya, R. Schwengner, S. Goriely, A. C. Larsen, D. M. Filipescu, I. Gheorghe, L. A. Bernstein, D. L. Bleuel, T. Glodariu, A. Görgen, M. Guttormsen, T. W. Hagen, B. V. Kheswa, Y.-W. Lui, D. Negi, I. E. Ruud, T. Shima, S. Siem, K. Takahisa, O. Tesileanu, T. G. Tornyi, G. M. Tveten, and M. Wiedeking, *Phys. Rev. C* **93**, 064302 (2016).
- [27] B. A. Brown and A. C. Larsen, *Phys. Rev. Lett.* **113**, 252502 (2014).
- [28] A. C. Larsen and S. Goriely, *Phys. Rev. C* **82**, 014318 (2010).
- [29] OXBASH (The Oxford-Buenos-Aires-MSU Shell Model Code), W. D. M. Rae, A. Etchegoyen, N. S. Godwin, and B. A. Brown, MSUCL Report Number 524 (1984).
- [30] W. Kutchera, B. A. Brown, and K. Ogawa, *Nuov. Cim.* **1**, No. 12 (1978).
- [31] R. Sen'kov and V. Zelevinsky, *Phys. Rev. C* **93**, 064304 (2016).
- [32] A. Bohr and B.R. Mottelson, *Nuclear Structure*, Vol. I: Single Particle Motion, p. 169 (W. A. Benjamin, INC, 1969).
- [33] M. Honma, T. Otsuka, B. A. Brown and T. Mizusaki, *Phys. Rev. C* **69**, 034335 (2004).
- [34] M. Honma, T. Otsuka, B. A. Brown and T. Mizusaki, *Eur. Phys. J. A* **25**, Suppl. 1, 499 (2005).
- [35] A.C. Larsen, private communication; re-analysis of data from A.C. Larsen *et al.*, Ref. [16].
- [36] Data measured at the Oslo Cyclotron Laboratory with the Oslo method, found in <http://www.mn.uio.no/fysikk/english/research/about/infrastructure/OCL/nuclear-physics-research/> compilation/.
- [37] V. Zelevinsky, B.A. Brown, N. Frazier, and M. Horoi, *Phys. Rep.* **276**, 85 (1996).
- [38] V.K.B. Kota, *Embedded Random Matrix Ensembles in Quantum Physics*, Lecture Notes in Physics, vol. 884 (Springer, Heidelberg, 2014).